Inorganic Chemistry

Article

pubs.acs.org/IC

Mo_2 Paddlewheel Complexes Functionalized with a Single MLCT, S_1 Infrared-Active Carboxylate Reporter Ligand: Preparation and Studies of Ground and Photoexcited States

Samantha E. Brown-Xu, Malcolm H. Chisholm,* Christopher B. Durr, Sharlene A. Lewis, Thomas F. Spilker, and Philip J. Young

Department of Chemistry and Biochemistry, The Ohio State University, 100 W. 18th Avenue, Columbus, Ohio 43210, United States

Supporting Information

ABSTRACT: From the reactions between $Mo_2(DAniF)_3$pivalate (DAniF = *N*,*N*′-di(*p*-anisyl)formamidinate) and the carboxylic acids LH, the title compounds $Mo_2(DAniF)_3L$ have been prepared and characterized: compounds **I** (L = $O_2CC{\equiv}CPh$), **II** (L = $O_2CC_4H_2SC{\equiv}CH$), and **III** (L = $O_2CC_6H_4$-*p*-CN). The new compounds have been characterized in their ground states by spectroscopy (^{1}H NMR, ultraviolet−visible absorption, near-infrared absorption, and steady state emission), cyclic voltammetry, and density functional theory calculations. The compounds show strong metal Mo_2 to ligand L $\delta-\pi^*$ transitions in their visible spectra. The nature of the S_1 ^{1}MLCT and T_1 states has been probed by time-resolved (femtosecond and nanosecond) transient absorption and infrared spectroscopy. The observed shifts of the C≡C and C≡N vibrational modes are found to be consistent with the negative charge being localized on the single L in the S_1 states, while the T_1 states are $^3Mo_2$ $\delta\delta^*$. The present results are compared to earlier studies of the photoexcited states of *trans*-Mo_2(2,4,6-triisopropylbenzoate)$_2L_2$ compounds that have been assigned as either localized or delocalized.

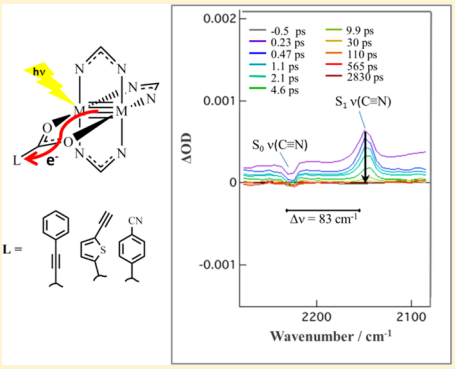

INTRODUCTION

Photoinduced metal-to-ligand charge transfer (MLCT) is fundamental to life in seemingly innumerable ways.[1] Of particular current interest are applications in the areas of photovoltaics, photocatalysis, and photoluminescence.[2−6] Carboxylate ligands attached to metal-to-metal (MM) quadruply bonded centers exhibit strong MM-to-ligand $\delta-\pi^*$ transitions that can be tuned to span the entire visible region of the spectrum and well into the near-infrared (NIR) region (400−1200 nm) by the appropriate selection of MM (MM = Mo_2, MoW, or W_2) and carboxylate.[7,8] Interestingly, the photoexcited states have relatively long S_1 lifetimes, 1−20 ps, before intersystem crossing leads to T_1 states that for Mo_2 complexes are typically $^3Mo_2$ $\delta\delta^*$ but for W_2 complexes are ^{3}MLCT. This has allowed us to probe both the S_1 and T_1 states, where S_1 and T_1 are the lowest-energy singlet and triplet excited states, respectively, by time-resolved femtosecond and nanosecond spectroscopies and to monitor how charge delocalization changes with time. We have previously examined compounds of the general formula *trans*-$M_2L_2L_2'$, where L′ is 2,4,6-triisopropylbenzoate (T*i*-PrB) and L is a π-acceptor ligand, or where L′ is acetate and L is *i*-PrNC(C≡CR)N*i*-Pr.[9−11] In these complexes, the lowest-energy singlet state is ^{1}MLCT and involves the π-acceptor ligands L. This immediately raises the question of whether the negative charge is localized on one ligand or delocalized over both. These can be viewed as valence-trapped or delocalized excited-state mixed valence complexes, respectively.[12] We sought to answer these questions by incorporating ligands containing IR-active C≡X groups (X = C or N) and measuring the shift in ν(C≡X) in the excited states and by performing calculations on the neutral complex and on a singly reduced species in which the formal negative charge is delocalized over both ligands. A more obvious and practical comparison lies in examining the excited states of molecules having only one π-acceptor ligand, and we herein report studies prompted by this consideration.

RESULTS AND DISCUSSION

Syntheses. Compounds of the form *trans*-Mo_2(T*i*-PrB)$_2L_2$ have previously been prepared from the reactions between Mo_2(T*i*-PrB)$_4$ and 2 equiv of the carboxylic acids LH. Cis−trans isomerization is not known to occur in these compounds,[13] and preparation of *cis*-carboxylates requires a different methodology.[14] Therefore these trans-substituted complexes appear to represent a thermodynamic product as a result of both relief of strain, which is present in the sterically crowded Mo_2(T*i*-PrB)$_4$ molecule, and of π-back bonding to the planar conjugated carboxylate ligands, as this geometry facilitates the ligand π-to-π coupling though the M_2 center. A prime example of this is seen in the structure of the *trans*-azulene carboxylate ester complex whose structure is seen in

Received: November 5, 2013
Published: December 20, 2013

Figure 1.[13] Here the planar structure of the two trans ligands is a result of the W_2-to-ligand $\delta-\pi^*$ conjugation. In previous

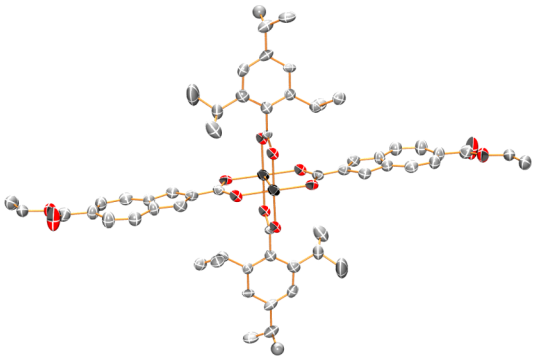

Figure 1. Molecular representation of *trans*-W_2(T*i*-PrB)$_2L_2$, where L = 6-carboethoxy-2-azulene carboxylate in the solid state.[19] Thermal ellipsoids are drawn at the 50% probability level. Hydrogens have been removed for clarity. Black = tungsten; scarlet = oxygen; gray = carbon.

work, we observed that if 1 equiv of a carboxylic acid is allowed to react with Mo_2(T*i*-PrB)$_4$, only the bis-substituted product is obtained.[15] The preparation of a related M_2(T*i*-PrB)$_3$L complex is thus not favored on either thermodynamic or kinetic grounds, as the carboxylate ligands are labile and prone to ligand scrambling.[16,17] In the present case, we have employed as the starting material a complex with one labile carboxylate and three kinetically persistent formamidinate ligands, Mo_2(DAniF)$_3$(piv), where DAniF = *N*,*N*′-di(*p*-anisyl)-formamidinate and piv = pivalate. A similar compound, Mo_2(DAniF)$_3$(O_2CCH_3), was employed by Cotton, Murillo, and co-workers in reactions with dicarboxylic acids leading to linked dinuclear compounds.[18] The reaction leading to the compounds is shown in eq 1 below (THF = tetrahydrofuran).

$$Mo_2(DAniF)_3(piv) + LH \xrightarrow[THF]{25^\circ C} Mo_2(DAniF)_3L + pivH \quad (1)$$

The new compounds **I**, **II**, and **III**, where L = $O_2CC{\equiv}CPh$, $O_2CC_4H_2SC{\equiv}CH$, and $O_2CC_6H_4$-p-C≡N, respectively, are orange (**I**), orange-red (**II**), and purple (**III**) crystalline solids that are soluble in toluene and polar solvents such as THF, dimethyl sulfoxide (DMSO), and CH_2Cl_2. They show molecular ions in the matrix-assisted laser desorption time-of-flight mass spectrometry (MALDI-TOF MS), and ^{1}H NMR and other characterization data are summarized in the Experimental Section.

Single Crystal and Molecular Structure of III (L = $O_2CC_6H_4$-*p*-C≡N). A view of the *p*-cyanobenzoate derivative **III** in its molecular form as seen in the solid state is shown in Figure 2. This confirms the expected paddle-wheel structure and the presence of a single carboxylate ligand. The dihedral angle between the O_2C and C_6H_4 plane is ∼18°, which allows for the Mo_2-to-ligand $\delta-\pi^*$ conjugation. The metric parameters are given in the Supporting Information (Table S1) and are typical for a quadruply bonded Mo_2^{4+} unit.[20]

Electronic Structure Calculations. To aid in the interpretation of the spectroscopic data, vide infra, we have carried out calculations on the model compounds Mo_2(HNC(H)NH)$_3$L. The substitution of NH for *N*-*p*-anisole reduces computational time, and the results of the calculations reflect the trends expected as a function of the carboxylate ligands L. The model compounds of **I**, **II**, and **III** are denoted as **I**′, **II**′, and **III**′, respectively. The HOMO in each compound is principally the Mo_2 δ orbital but with significant mixing of the ligands. In comparison to tetracarboxylate complexes the Mo_2 δ orbital is raised in energy by ∼1 eV. The amidinate ligands are higher in energy because of the less electronegative nature of nitrogen relative to oxygen. This results in greater mixing of the filled NCN π-orbitals with the Mo_2 δ orbital. A similar effect is also seen on the Mo_2 δ^* orbital, which again is notably higher in energy because of interaction with the NCN nonbonding orbital. Below the HOMO-1, which is a filled NCN π combination, are the Mo_2 π and L π orbitals that are close in energy. In all cases, the LUMO is principally carboxylate ligand π^* in character, and the LUMO+1 is an orbital which has both Mo_2 σ^* and 5s character. The LUMO+2 is the Mo_2 δ^* orbital. The HOMO−LUMO gap follows the order of ligands such that the gap is largest for L = $O_2CC{\equiv}CPh$ and smallest for L = $O_2CC_6H_4C{\equiv}N$. Thus the lowest-energy electronic transition is primarily a fully allowed Mo_2-to-ligand $\delta-\pi^*$ ^{1}MLCT transition that readily accounts for the colors of compounds **I** (orange), **II** (orange-red), and **III** (purple).

The frontier molecular orbital energies for the model compounds are shown in Figure 3 along with the GaussView isosurface contour plots for the cyanobenzoate. The LUMOs of the three compounds are shown in Figure 4 to more clearly represent the nature of the L π^* orbitals.

Electronic Absorption and Steady State Emission Spectra. The ultraviolet−visible (UV−vis) spectra of

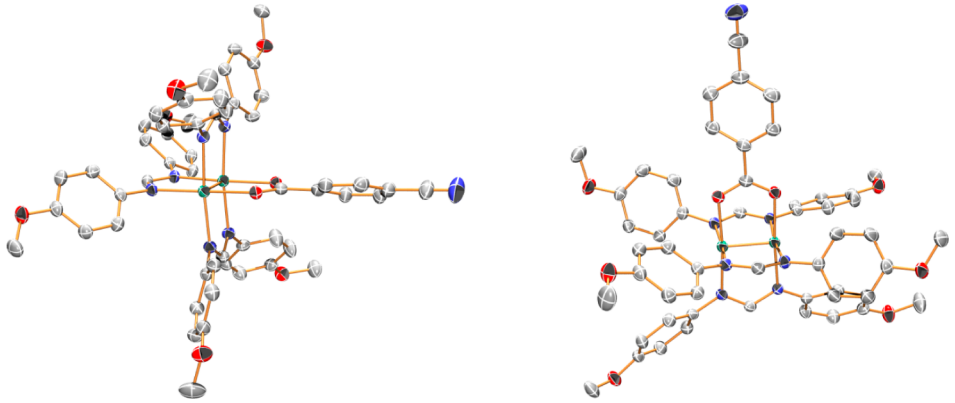

Figure 2. Two views of the molecular structure of compound **III** in the solid state. Thermal ellipsoids are drawn at the 50% probability level. Hydrogens have been removed for clarity. Teal = molybdenum; blue = nitrogen; scarlet = oxygen; gray = carbon.

dx.doi.org/10.1021/ic402775s | *Inorg. Chem.* 2014, 53, 637−644

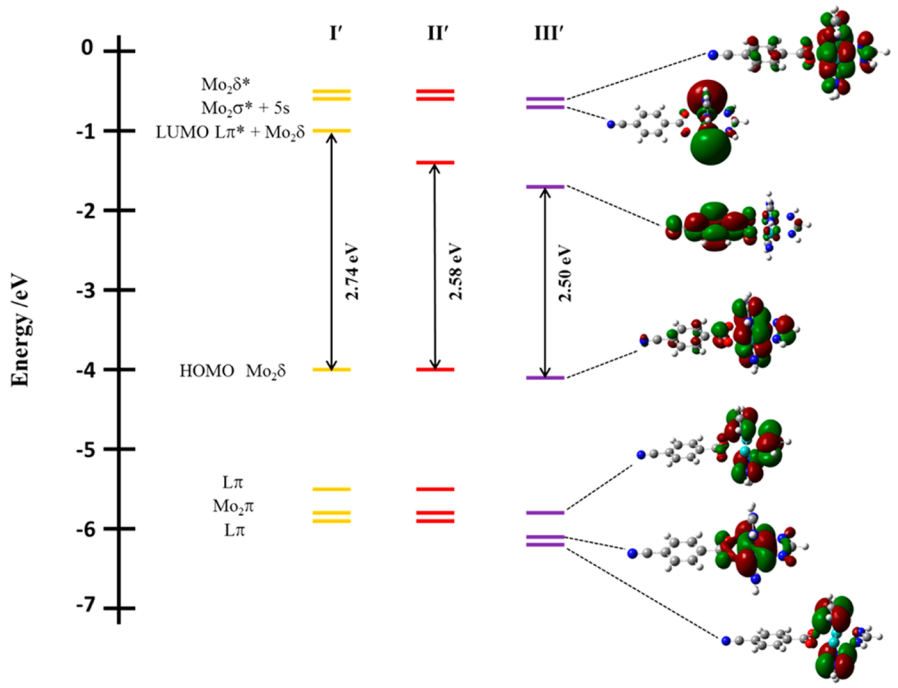

Figure 3. Frontier orbital energy diagram comparing **I′**, **II′**, and **III′**. GaussView 5.0.8 isosurface contour plots for the molecular orbitals of **III′** are also shown.

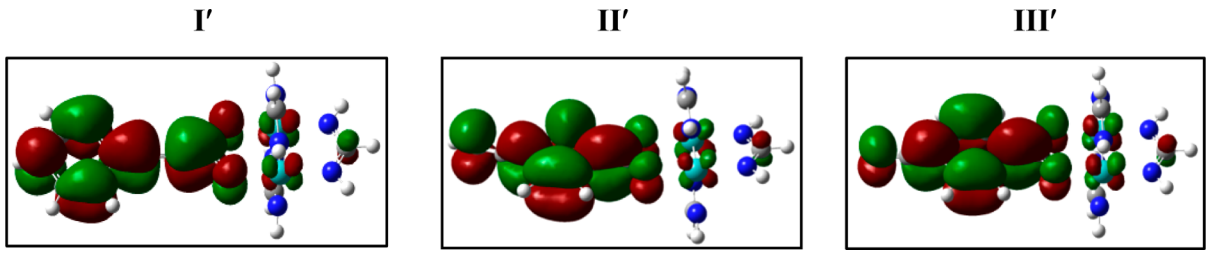

Figure 4. GaussView 5.0.8 contour plots of the LUMO of model compounds **I′**, **II′**, and **III′**.

$Mo_2(DAniF)_3(piv)$ and compounds **I**, **II**, and **III** are shown in Figure 5, and the calculated λ_{max} from time-dependent density functional theory (TD-DFT) calculations are compared with the observed λ_{max} values for compounds **I**, **II**, and **III** in Table 1. The calculated values pertain to molecules with O_2C-ring

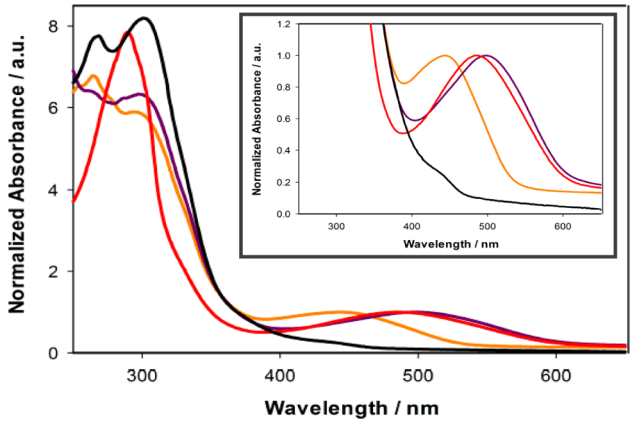

Figure 5. Absorption spectra of $Mo_2(DAniF)_3(piv)$ (black) and **I** (orange), **II** (red), and **III** (purple) in THF. An expanded view of the MLCT absorption bands is presented in the inset.

Table 1. λ_{max} of Calculated and Observed MLCT Absorption Band for Compounds I, II, and III

compound	calculated λ_{max}, nm	observed λ_{max}, nm
I	516	444
II	558	488
III	568	498

dihedrals of 0°, which thus maximizes the degree of Mo_2-to-ligand $\delta-\pi^*$ overlap and lowers the energy of the HOMO–LUMO gap to a minimum. In solution at room temperature there will be a Boltzmann distribution of O_2C–Ar dihedral angles with a weighted average of 0°. It is thus not surprising that the calculated λ_{max} are somewhat red-shifted when compared to the observed.

Note that the intensities of these MLCT transitions are notably less than those seen for compounds of the form *trans*-$Mo_2(Ti\text{-}PrB)_2L_2$. It is reasonable to assume that, to a first approximation, the intensity of the MLCT correlates inversely with the energy gap of the interacting orbitals but is directly proportional to the degree of overlap of the same.[21,22] Therefore in these formamidinate complexes the mixing of the NCN π system with the Mo_2 δ orbital decreases the interaction between the Mo_2 δ and the CO_2 π system relative to compounds of the form $Mo_2(O_2CR)_4$. This reduced orbital

dx.doi.org/10.1021/ic402775s | Inorg. Chem. 2014, 53, 637–644

overlap results in the observed decrease in intensity in the MLCT transition.

The complexes show very weak singlet emission at room temperature but emit strongly from the T_1 states. All of the new compounds show phosphorescence at ~860 nm (Supporting Information, Figure S1), as does $Mo_2(DAniF)_3(piv)$, which we assign to emission from the $^3Mo_2$ $\delta\delta^*$ state due to the ligand independence of the emission. This is notably higher in energy relative to that seen in Mo_2 tetracarboxylates as a result of the greater mixing of the Mo_2 δ and δ^* orbitals with the filled NCN π orbitals. DFT calculations indicate that the lowest-energy triplet state is $^3Mo_2$ $\delta\delta^*$ in nature. The fluorescence spectra for compounds **I**, **II**, and **III** (Figure 6) can be readily assigned to

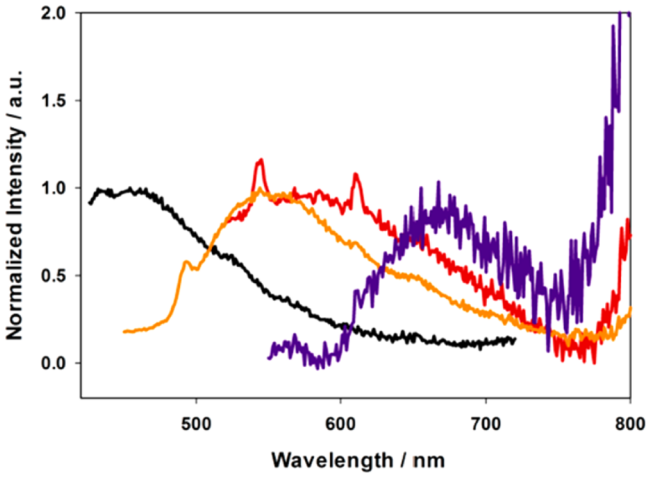

Figure 6. Fluorescence spectra of $Mo_2(DAniF)_3(piv)$ (black) and compounds **I** (orange), **II** (red), and **III** (purple) in THF at room temperature.

emission from the ^{1}MLCT state; however, for the pivalate complex we present evidence, vide infra, that the S_1 state is likely $^1Mo_2$ $\delta\delta^*$, as was seen in $Mo_2(piv)_4$.[23]

Cyclic Voltammetric Studies. In THF, all three compounds show a quasi-reversible oxidation wave between −0.15 and −0.29 V relative to the $FeCp_2^{0/+}$ couple assignable to the removal of an electron from the Mo_2 δ orbital. The $E_{1/2}$ values are notably shifted to lower potential when compared with their *trans*-$Mo_2(Ti\text{-}PrB)_2L_2$ counterparts, as expected on the basis of the calculations. Oxidation of the formamidinate ligands occurs at higher potentials (~0.60 V). No reversible reduction waves were assigned within the solvent window, though for compound **II** an irreversible wave appears. The electrochemical data are summarized in Table 2.

Time-Resolved Spectroscopic Studies. *Time-Resolved Infrared Spectroscopy.* The four compounds have been examined by femtosecond time-resolved infrared (TRIR) spectroscopy in the window of 2300−1350 cm^{-1} to learn how charge distribution changes in the excited states. Ground-state IR spectra can be found in the Supporting Information (Figure S2) as well as in the TRIR spectra. The spectra of $Mo_2(DAniF)_3(piv)$ (Figure 7) provide a benchmark for compounds **I**, **II**, and **III** and are described first.

Table 2. Summary of Electrochemical Data for Compounds I, II, and III[a]

compound	$E^{ox}_{1/2}$, V	E^{red}, V
I	−0.15, 0.68	
II	−0.29	−2.66
III	−0.18, 0.61	

[a]Potentials are referenced to the $FeCp_2^{+/0}$ couple. Data obtained in THF at room temperature.

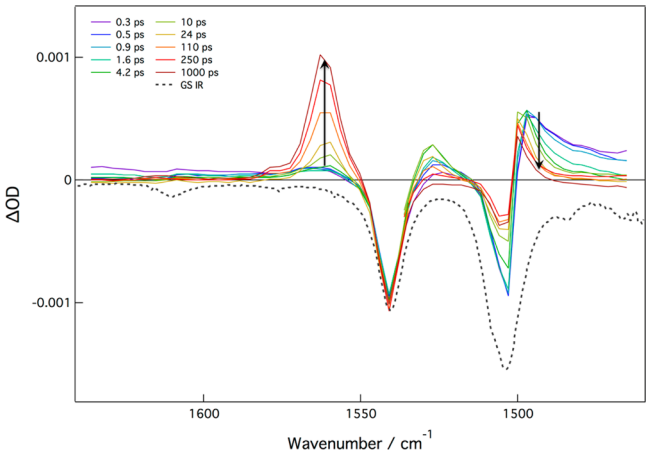

Figure 7. Femtosecond TRIR spectra of $Mo_2(DAniF)_3(piv)$ in THF at room temperature (RT), λ_{ex} = 400 nm. The ground-state IR spectrum is shown in the dashed line.

The principal features in the spectra of $Mo_2(DAniF)_3(piv)$ occur from 1600 to 1450 cm^{-1}, where the $\nu_{as}(CO_2)$ and $\nu_{as}(CN_2)$ vibrational modes in the ground and excited states are found. Initially, bleaches of the $\nu_{as}(CN_2)$ and $\nu_{as}(CO_2)$ modes are seen at 1540 and 1500 cm^{-1}, respectively, along with a transient absorption at 1490 cm^{-1} that is assignable to $\nu_{as}(CO_2)$ in the ^{1}MLCT (S_2) state . A weak signal assignable to $\nu_{as}(CN_2)$ is observed at higher energy relative to its position in the ground state. Within 5 ps, the $\nu_{as}(CO_2)$ band begins to shift to higher energy, and a new band appears at ~1525 cm^{-1}. These features are evidence of the formation of the $^1Mo_2$ $\delta\delta^*$ state from the ^{1}MLCT state, which was observed previously in $Mo_2(piv)_4$.[23] Finally, over 70 ps, a $\nu_{as}(CN_2)$ band at 1560 cm^{-1} grows in while $\nu_{as}(CO_2)$ shifts to slightly higher energy. These longer-lived features can reliably be associated with the $^3Mo_2$ $\delta\delta^*$ state formed following intersystem crossing from $^1Mo_2$ $\delta\delta^*$.

Interestingly, in these tris-formamidinate complexes it is the $\nu_{as}(CN_2)$ stretch that is shifted to higher energy rather than the $\nu_{as}(CO_2)$ stretch, as was seen for $Mo_2(piv)_4$.[23] Removal of an electron from a δ orbital will reduce the degree of back-bonding to the ligands and may contribute to the above observations. In any event the calculations on the T_1 state of this molecule predict this relative positioning of the vibrations in the triplet state. Similar long-lived features are seen for the other compounds characteristic of a $^3Mo_2$ $\delta\delta^*$ T_1 state, though bands due to a $^1Mo_2$ $\delta\delta^*$ state are not observed for **I**, **II**, or **III** since the S_1 state is ^{1}MLCT. In these complexes, however, the main focus is examining the magnitude of the shift of $\nu(C{\equiv}X)$ from the ground state to the ^{1}MLCT state in which electron density resides on the one carboxylate ligand.

For compound **I**, where L = $O_2CC{\equiv}CPh$, the femtosecond TRIR spectra (Figure 8) in the higher-energy region display weak features due to the $\nu(C{\equiv}C)$ in the S_1 state at ~1980 cm^{-1}. When compared to the ground-state IR spectrum (Supporting Information, Figure S2) this reflects a substantial shift to lower energy ($\Delta\nu(C{\equiv}C)$ = −245 cm^{-1}) and is in

dx.doi.org/10.1021/ic402775s | Inorg. Chem. 2014, 53, 637−644

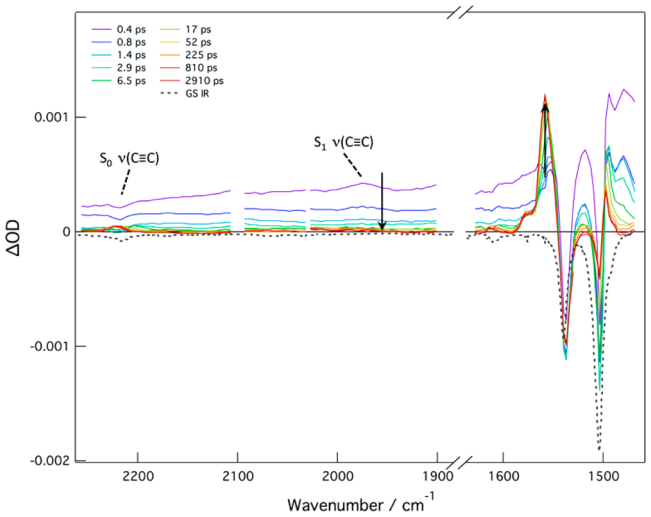

Figure 8. Femtosecond TRIR spectra of **I** in THF at RT, λ_{ex} = 400 nm. The ground-state IR spectrum is shown in the dashed line.

agreement with previously studied compounds which were assigned as having localized ^{1}MLCT states. Namely, the compounds *trans*-$W_2(T\textit{i}\text{-PrB})_2(O_2CC{\equiv}CC_6H_4CH_3)_2$ and *trans*-$Mo_2(O_2CMe)_2[(Pr^iN)_2CC{\equiv}CPh]_2$ both showed a prominent C≡C stretch in their ^{1}MLCT states shifted −240 cm^{-1} from the ground-state vibration.[11,24] In contrast, the compound *trans*-$Mo_2(T\textit{i}\text{-PrB})_2(O_2CC{\equiv}$C-9-anthracene$)_2$ gave a $\Delta\nu$(C≡C) of only −90 cm^{-1} and in this case was assigned as a delocalized ^{1}MLCT state with the negative charge shared by both trans ligands.[24] For **I**, the ^{1}MLCT state decays (τ = 2 ps) to form the $^3Mo_2$ $\delta\delta^*$ state that shows evidence of ν(C≡C) shifted to a slightly higher energy relative to the ground state.

The TRIR spectra for compound **II** (Figure 9) show the appearance of a weak absorption band at 1970 cm^{-1} because of

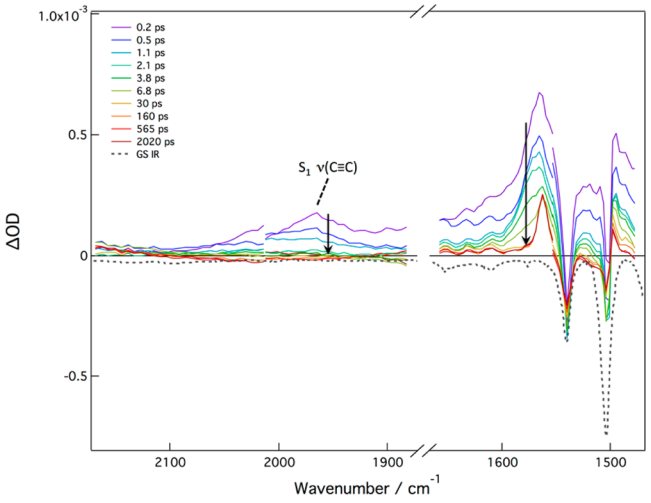

Figure 9. Femtosecond TRIR spectra of compound **II** in THF at RT, λ_{ex} = 515 nm. The ground-state IR spectrum is shown in the dashed line.

ν(C≡C) in the ^{1}MLCT state. This is shifted ∼130 cm^{-1} to lower energy relative to the ground state. This shift is twice the magnitude of $\Delta\nu$(C≡C) of the related compound *trans*-$Mo_2(T\textit{i}\text{-PrB})_2(O_2CC_4H_2SC{\equiv}CH)_2$ that has two conjugated carboxylate ligands and was assigned as a delocalized ^{1}MLCT.[25]

Again, following S_1 decay (τ = 4.5 ps), the $^3Mo_2$ $\delta\delta^*$ state is formed as denoted by the characteristic features from 1500 to 1600 cm^{-1}.

The TRIR spectra for the cyanobenzoate complex **III** are shown in Figure 10. The higher-energy region displays the

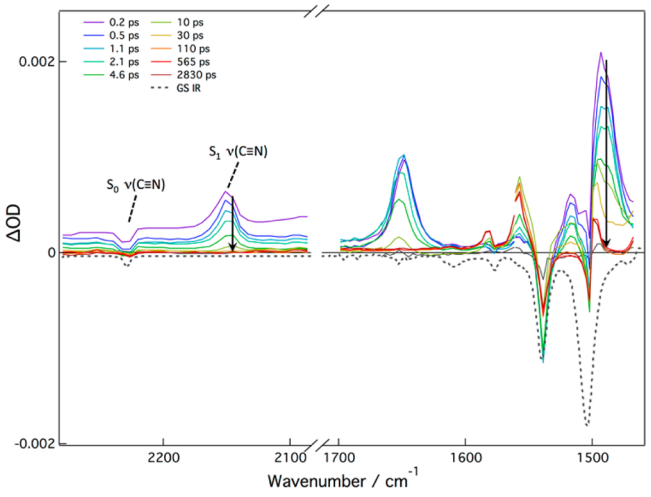

Figure 10. Femtosecond TRIR spectra of compound **III** in THF at RT, λ_{ex} = 568 nm. The ground-state IR spectrum is shown in the dashed line.

bleach of the ground state ν(C≡N) at 2232 cm^{-1} and the appearance of the singlet excited state ν(C≡N) at 2148 cm^{-1}, shifted 84 cm^{-1} from the ground state. The change in the C≡N vibration is again greater than that observed for the corresponding complex with two cyanobenzoate ligands, *trans*-$Mo_2(T\textit{i}\text{-PrB})_2(O_2CC_6H_4C{\equiv}N)_2$,[11] consistent with the previous assignment of a delocalized ^{1}MLCT state. In the present case, however, there is a new band visible at 1655 cm^{-1} that appears to be at a higher energy relative to ground-state ligand modes. This vibration we assign to ν(C═C) of a ring mode associated with the quinoidal nature of the excited state as depicted below.

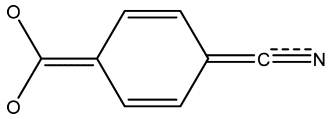

These features disappear after singlet state decay (τ = 5 ps) in accordance with formation of a metal-based T_1 state. The values of ν(C≡X) in the present compounds are compared with those in the related *trans*-$Mo_2L_2L_2'$ compounds in Table 3 along with the values of $\Delta\nu$(C≡X) and those calculated for the anions.

Transient Absorption Spectroscopy. The compounds have been examined in THF solutions by both femtosecond and nanosecond transient absorption (TA) spectroscopy, which has allowed us to correlate the lifetimes of their excited states with those estimated from the TRIR studies. The lifetimes for compounds **I** and **II** agree well, and the TA spectra can be found in the Supporting Information (Figures S4, S5, S8, and S9). However, the TA spectra of $Mo_2(DAniF)_3(piv)$ and compound **III** warrant discussion.

The TA spectra for the pivalate complex in the region 350−650 nm are shown in Figure 11. At ∼350 nm we see the expected bleach associated with the ^{1}MLCT. At short times less than 5 ps, we observe the appearance of an absorption band at

dx.doi.org/10.1021/ic402775s | Inorg. Chem. 2014, 53, 637−644

Table 3. Summary of ν(C≡X) and $\Delta\nu$(C≡X) Values

	experimental, cm^{-1}			calculated, cm^{-1}
	ground state	^{1}MLCT state	shift	shift in anion
compound	ν(C≡C)	ν(C≡C)*	$\Delta\nu$(C≡C)	$\Delta\nu$(C≡C)
I	2220	1975	240	*a*
$Mo_2(O_2CMe)_2[(Pr^iN)_2CC{\equiv}C\text{-}Ph]_2$ [b]	2200	2155, 1959	45, 241	141
$Mo_2(Ti\text{-}PrB)_2(O_2CC{\equiv}C\text{-}9\text{-}An)_2$ [c]	2204	2113	91	101
II	2100	1970	130	155
$Mo_2(Ti\text{-}PrB)_2(O_2CC_4H_2SC{\equiv}CH)_2$ [d]	2099	2033	66	57
	ν(C≡N)	ν(C≡N)*	$\Delta\nu$(C≡N)	$\Delta\nu$(C≡N)
III	2230	2145	85	112
$Mo_2(Ti\text{-}PrB)_2(O_2CPhC{\equiv}N)_2$ [e]	2230	2157	73	67

[a]Calculation on the anion returned with a negative frequency. [b]Values from ref 11; localized ^{1}MLCT. [c]Values from ref 17; An = anthracenyl; delocalized ^{1}MLCT. [d]Values from ref 18; delocalized ^{1}MLCT. [e]Values from ref 11; delocalized ^{1}MLCT.

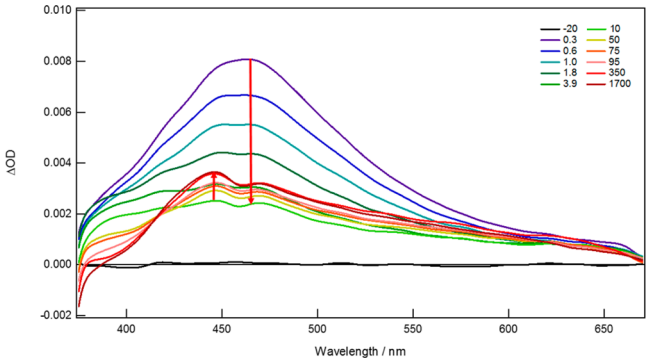

Figure 11. Femtosecond TA spectra of $Mo_2(DAniF)_3(piv)$ in THF at RT, λ_{ex} = 350 nm.

460 nm. This early transient is assigned to the ^{1}MLCT state that decays to the $^1Mo_2$ $\delta\delta$* state. A feature at 440 nm, because of the decay of the $^1Mo_2$ $\delta\delta$* state into the long-lived $^3Mo_2$ $\delta\delta$* state, grows in over 70 ps. This lifetime is comparable to that seen for the homoleptic compound $Mo_2(piv)_4$.[23] The isosbestic point observed at 410 nm indicates direct conversion from the singlet to the triplet $\delta\delta$* state. The nanosecond TA spectrum is given in the Supporting Information (Figure S7) from which we can reasonably estimate the lifetime of the T_1 $^3Mo_2$ $\delta\delta$* state to be ~70 μs.

The femtosecond TA spectra for the *para*-cyanobenzoate complex **III** are shown in Figure 12. The bleach of the ^{1}MLCT occurs from 450 to 525 nm. At lower energy, namely ~660 nm, there is a negative feature that is not reconcilable with the ^{1}MLCT absorption but rather with stimulated emission from

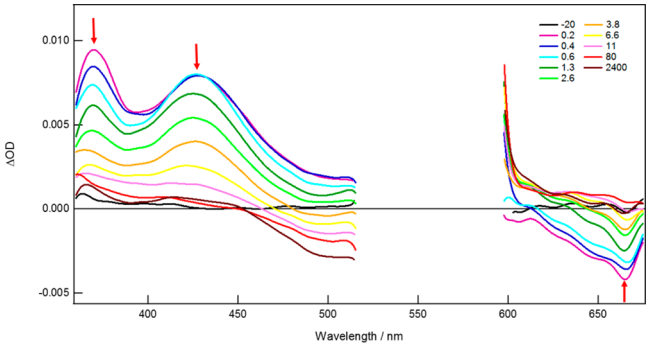

Figure 12. Femtosecond TA spectra of compound **III** in THF at RT, λ_{ex} = 568 nm.

the ^{1}MLCT state (τ = 3 ps), consistent with the decay of the transient seen at 365 nm. There is also clearly a band at 430 nm that shows a different kinetic decay. We propose that this arises from an $S_1 \rightarrow S_m$ absorption that differs from the $S_1 \rightarrow S_n$ absorption ($n > m$) at 365 nm. Within 5 ps this transient decays to leave the longer-lived features associated with the T_1 state. From the nanosecond TA spectra shown in the Supporting Information (Figure S10) the lifetime of the T_1 $^3Mo_2$ $\delta\delta$* state is estimated to be ~75 μs.

CONCLUSIONS

Studies of Mo_2 complexes with a single IR-active group (C≡X) provide a way to experimentally evaluate charge distribution in excited states. Monofunctionalized complexes possess fully localized excited states, which can be used to model electron delocalization in higher-order systems. The shift of ν(C≡X) in the ^{1}MLCT states of **I**, **II**, and **III** are roughly twice the magnitude of those seen for related *trans*-$Mo_2(Ti\text{-}PrB)_2(O_2CR)_2$ compounds that have been assigned as delocalized ^{1}MLCT states. This supports our earlier assignments of delocalized and localized excited states. The presence of the three formamidinate ligands raises the energy of the Mo_2 δ orbital relative to that of the tetracarboxylate complexes. This is clearly seen in the electrochemistry and also in the emission from the $^3Mo_2$ $\delta\delta$* state, which moves to higher energy. Finally, we note here that the time-resolved spectra for the complex $Mo_2(DAniF)_3(piv)$ indicate that the S_1 is $^1Mo_2$ $\delta\delta$* as was found for $Mo_2(piv)_4$. Interestingly, internal conversion between the ^{1}MLCT state and the $^1Mo_2$ $\delta\delta$* state, which are close in energy, is sufficiently slow that the former can be detected by femtosecond spectroscopies.

EXPERIMENTAL SECTION

General Procedures. The Mo_2 complexes were prepared under an inert atmosphere (argon or nitrogen) using standard glovebox and Schlenk line techniques. Solvents were dried using standard methods and degassed before use if needed. Phenylpropiolic acid and *p*-cyanobenzoic acid were purchased from Sigma Aldrich. $Mo_2(piv)_4$[26] and 5-ethynylthiophene-2-carboxylic acid[27] were prepared by reported procedures. $Mo_2(DAniF)_3(piv)$ was prepared using an adapted procedure in which $Mo_2(piv)_4$ was used instead of $Mo_2(O_2CCH_3)_4$.[18] The ^{1}H NMR spectra were recorded on a 400 MHz Bruker DPX Advance 400 spectrometer. All ^{1}H NMR chemical shifts are in ppm relative to the protio impurity in THF-d_8 at 3.58 ppm or DMSO-d_6 at 2.50 ppm.

dx.doi.org/10.1021/ic402775s | *Inorg. Chem.* 2014, 53, 637−644

Electronic Absorption Spectra. UV−vis-NIR electronic spectra were measured in THF at room temperature with a Perkin-Elmer Lambda 900 spectrometer using 1 cm^2 quartz cuvettes sealed with Kontes taps.

Electrochemical Studies. Cyclic voltammograms were collected at a scan rate of 100 mV s^{-1} with a Pine Research Instrumentation Wavenow potentiostat−galvanostat. The measurements were performed under a nitrogen atmosphere in a 0.1 M THF solution of the supporting electrolyte tetra-*n*-butylammonium hexafluorophosphate using platinum working and auxiliary electrodes patterned on ceramic and a silver wire pseudo reference electrode (Pine Research Instrumentation). The potentials are referenced to the $FeCp_2^{+/0}$ couple.

Mass Spectrometry. The MALDI-TOF mass spectrometry experiments were performed on a Bruker Microflex mass spectrometer. Dithranol was employed as the matrix.

Electronic Structure Calculations. Utilizing the Gaussian09 suite of programs, DFT was used for the gas-phase optimization of the model complexes.[28,29] The B3LYP[30,31] functional was used together with the SDD energy-consistent pseudopotentials and the SDD energy-consistent basis set for molybdenum, and the 6-31G* basis set was used for H, C, N, S, and O atoms. Vibrational frequency analysis was used to ensure that the optimized structures represented global minima on the potential energy surface. GaussView 5.0.8 isosurface contour plots are shown with an isovalue of 0.02.[31] Electronic absorption spectra were calculated using the TD-DFT method with the same functional and basis set used for DFT calculations.

Crystallographic Information. Single crystals of **III** were isolated as prismatic dark-purple crystals and handled under a pool of fluorinated oil. Examination of the diffraction pattern was done on a Nonius Kappa CCD diffractometer with Mo Kα radiation. All work was done at 150 K using an Oxford Cryosystems Cryostream Cooler. Data integration was done with Denzo, and scaling and merging of the data was done with SADABS.[32] The structures were solved by the direct methods program in SHELXS-13.[33] Full-matrix least-squares refinements based on F^2 were performed in SHELXL-13,[33] as incorporated in the WinGX package.[34] For each methyl group, the hydrogen atoms were added at calculated positions using a riding model with $U(H) = 1.5U_{eq}$ (bonded carbon atom). The rest of the hydrogen atoms were included in the model at calculated positions using a riding model with $U(H) = 1.2U_{eq}$ (bonded atom). Neutral atom scattering factors were used and include terms for anomalous dispersion.[35]

Time-Resolved Measurements. Femtosecond TA[36] and TRIR[37] spectroscopy experiments were performed with a Ti:sapphire and regenerative amplifier combination (1 kHz, 300 fs full width at half-maximum) that has been previously described. In the femtosecond TA experiment, samples were prepared with absorbances of ∼0.3−0.8 in a 1.0 mm quartz cuvette with Kontes top. Excitation power at the sample was 1−2 μJ. Spectra collected underwent wavelength calibration and group velocity dispersion corrections. $Mo_2(DAniF)_3(piv)$ and compounds **I**, **II**, and **III** were excited at 350, 514, 514, and 568 nm, respectively. In the femtosecond TRIR experiment, samples were prepared in THF with an absorbance of ∼1 at λ_{max}. The solutions were sealed in a PerkinElmer semi-demountable cell with a 0.1 mm Teflon spacer between 4 mm CaF_2 windows. $Mo_2(DAniF)_3(piv)$ and compounds **I**, **II**, and **III** were excited at 400, 400, 515, and 568 nm, respectively, with a laser power of ∼1 μJ. In the nanosecond TA experiment, samples were prepared in a 1 cm quartz cuvette with Kontes top with absorbance in the range of 0.1−0.3. Excitation power at the sample was 100 mW.[38] All samples were excited at a wavelength of 355 nm.

Kinetics for the time-resolved data was fit to a sum of exponentials $S(t) = \sum_i A_i \exp(-1/\tau_i) + C$, where A_i is the amplitude, τ_I is the lifetime, and C is an offset, in Igor Pro 6.0 or SigmaPlot 12.0. Standard errors of the exponential fits are given as the error bars of the lifetimes.

Steady State Emission Spectra. The steady-state luminescence spectra between 350 and 800 nm were acquired on a SPEX Fluoromax-2 spectrofluorometer. The spectra were measured in THF at room temperature and in 2-methyltetrahydrofuran at 77 K. Samples were excited into their MLCT bands. The steady-state near-IR luminescence spectra were taken on a home-built instrument utilizing a germanium detector. All measurements were recorded in 2-methyltetrahydrofuran with an excitation wavelength of 405 nm.

Preparation of $Mo_2(DAniF)_3(O_2CC{\equiv}CPh)$, I. THF (ca. 5 mL) was added to a mixture of $Mo_2(DAniF)_3(piv)$ (0.151 g, 0.143 mmol) and phenylpropiolic acid (0.0235g, 0.161 mmol). An orange solution was immediately formed. This was stirred at room temperature for 1 week. The solution was concentrated, and hexanes were added to precipitate the orange product. The mixture was washed once with ethanol and once with hexanes. The residue was dried under vacuum to yield an orange powder. Yield: 35%. ^{1}H NMR (THF-d_8, 400 MHz): 8.61 (s, 2H), 8.41 (s, 1H), 7.66 (d, 2H), 7.42 (d, 2H), 6.68 (d, 8H), 6.59 (d, 8H), 6.46 (d, 4H), 6.39 (d, 4H), 3.78 (s, 12H), 3.72 (s, 6H). MALDI-TOF: Calculated: 1102.9 Found: 1103.8. UV−vis (THF, nm): 444, 264.

Preparation of $Mo_2(DAniF)_3(O_2CC_4H_2SC{\equiv}CH)$, II. THF (ca. 5 mL) was added to a mixture of $Mo_2(DAniF)_3(piv)$ (0.131 g, 0.124 mmol) and 5-ethynylthiophene-2-carboxylic acid (0.028 g, 0.184 mmol). A red-orange solution was immediately formed. This was stirred at room temperature for 1 week. The solution was concentrated and hexanes were added to precipitate the red-orange product. The mixture was washed once with ethanol and once with hexanes. The residue was dried under vacuum to yield a red-orange powder. Yield: 51%. ^{1}H NMR (DMSO-d_6, 400 MHz): 8.55 (s, 1H), 8.43 (s, 2H) 7.65 (d, 2H), 7.42 (d, 2H), 6.68 (d, 8H), 6.59 (d, 8H), 6.46 (d, 4H), 6.39 (d, 4H), 3.66 (s, 12H), 3.61 (s, 6H). MALDI-TOF: Calculated: 1108.9 Found: 1107.3. UV−vis (THF, nm): 488, 289.

Preparation of $Mo_2(DAniF)_3(O_2CC_6H_4$-p-$C{\equiv}N)$, III. THF (ca. 5 mL) was added to mixture of $Mo_2(DAniF)_3(piv)$ (0.1664 g, 0.157 mmol) and *p*-cyanobenzoic acid (0.0249 g, 0.169 mmol). A red-purple solution was immediately formed. This was stirred at room temperature for 4 days. The solution was concentrated and hexanes (ca. 5 mL) and ethanol (ca. 5 mL) were added to precipitate the purple product. The mixture was washed once with ethanol and once with hexanes. The residue was dried under vacuum to yield a purple powder. Yield: 61%. ^{1}H NMR (THF-d_8, 400 MHz): 8.53 (s, 2H), 8.52 (s, 1H), 8.41 (d, 2H), 7.83 (d, 2H), 6.67 (d, 8H), 6.62 (d, 8H), 6.47 (d, 4H), 6.36 (d, 4H), 3.70 (s, 12H), 3.65 (s, 6H). MALDI-TOF: Calculated: 1103.9 Found: 1102.6. UV−vis (THF, nm): 498, 297.

dx.doi.org/10.1021/ic402775s | *Inorg. Chem.* 2014, 53, 637−644

■ ASSOCIATED CONTENT

Supporting Information

Table of crystallographic information, NIR emission spectra, ground-state IR spectra, kinetic data for time-resolved IR spectroscopy measurements, femtosecond and nanosecond transient absorption spectra and associated kinetic traces. This material is available free of charge via the Internet at http://pubs.acs.org. CCDC 969746 contains the supplementary crystallographic data for this paper. These data can be obtained free of charge from The Cambridge Crystallographic Data Center via www.ccdc.cam.ac.uk/data_request/cif.

■ AUTHOR INFORMATION

Corresponding Author

*E-mail: chisholm@chemistry.ohio-state.edu.

Notes

The authors declare no competing financial interest.

■ ACKNOWLEDGMENTS

We thank the National Science Foundation for financial support from Grant No. 0957191 and the Ohio Super Computer Center for computational resources. We also acknowledge Professor Terry L. Gustafson and the Ohio State University Center for Chemical and Biophysical Dynamics for use of the laser systems and Professor Claudia Turro for use of instrumentation. S.E. Brown-Xu acknowledges support from the NSF GRFP.

■ REFERENCES

(1) Vlček, A., Jr. *Coord. Chem. Rev.* **1998**, *177*, 219−256.

(2) Tsuboyama, A.; Iwawaki, H.; Furugori, M.; Mukaide, T.; Kamatani, J.; Igawa, S.; Moriyama, T.; Miura, S.; Takiguchi, T.; Okada, S.; Hoshino, M.; Ueno, K. *J. Am. Chem. Soc.* **2003**, *125*, 12971−12979.

(3) Chisholm, M. H.; Epstein, A. J.; Gallucci, J. C.; Feil, F.; Pirkle, W. *Angew. Chem., Int. Ed.* **2005**, *44*, 6537−6540.

(4) Burdzinski, G. T.; Chisholm, M. H.; Chou, P.-T.; Chou, Y.-H.; Feil, F.; Gallucci, J. C.; Ghosh, Y.; Gustafson, T. L.; Ho, M.-L.; Liu, Y.; Ramnauth, R.; Turro, C. *Proc. Natl. Acad. Sci. U.S.A.* **2008**, *105*, 15247−15252.

(5) Takeda, H.; Ishitani, O. *Coord. Chem. Rev.* **2010**, *254*, 346−354.

(6) Wong, W.-Y.; Ho, C.-L. *Acc. Chem. Res.* **2010**, *43*, 1246−1256.

(7) Brown-Xu, S. E.; Chisholm, M. H.; Durr, C. B.; Lewis, S. A.; Naseri, V.; Spilker, T. F. *Chem. Sci.* **2013**, *4*, 2105−2116.

(8) Chisholm, M. H.; Gustafson, T. L.; Turro, C. *Acc. Chem. Res.* **2013**, *46*, 529−538.

(9) Brown, D. J.; Chisholm, M. H.; Gallucci, J. C. *Dalton Trans.* **2008**, 1615−1624.

(10) Alberding, B. G.; Chisholm, M. H.; Gustafson, T. L.; Liu, Y.; Reed, C. R.; Turro, C. *J. Phys. Chem. A* **2010**, *114*, 12675−12681.

(11) Alberding, B. G.; Chisholm, M. H.; Gallucci, J. C.; Ghosh, Y.; Gustafson, T. L. *Proc. Natl. Acad. Sci. U.S.A.* **2011**, *108*, 8152−8156.

(12) Plummer, E. A.; Zink, J. I. *Inorg. Chem.* **2006**, *45*, 6556−6558.

(13) Barybin, M. V.; Chisholm, M. H.; Patmore, N. J.; Robinson, R. E.; Singh, N. *Chem. Commun.* **2007**, 3652−3654.

(14) Cotton, F. A.; Liu, C. Y.; Murillo, C. A. *Inorg. Chem.* **2004**, *43*, 2267−2276.

(15) Chisholm, M. H.; Epstein, A. J.; Gallucci, J. C.; Feil, F.; Pirkle, W. *Angew. Chem., Int. Ed.* **2005**, *44*, 6537−6540.

(16) Cayton, R. H.; Chacon, S. T.; Chisholm, M. H.; Folting, K. *Polyhedron* **1993**, *12*, 415−422.

(17) Chen, H.; Cotton, F. A. *Polyhedron* **1995**, *14*, 2221−2224.

(18) Cotton, F. A.; Liu, C. Y.; Murillo, C. A.; Villagrán, D.; Wang, X. *J. Am. Chem. Soc.* **2003**, *125*, 13564−13575.

(19) Alberding, B. G.; Barybin, M. V.; Chisholm, M. H.; Gustafson, T. L.; Reed, C. R.; Robinson, R. E.; Patmore, N. J.; Singh, N.; Turro, C. *Dalton Trans.* **2010**, *39*, 1979−1984.

(20) *Multiple Bonds between Metal Atoms*, 3rd ed.; Cotton, F. A.; Murillo, C. A.; Walton, Richard A., eds.; Springer Science and Business Media, Inc.: New York, 2005.

(21) Mulliken, R. S. *J. Am. Chem. Soc.* **1952**, *74*, 811−824.

(22) Turro, N. J.; Ramamurthy, V.; Gallucci, J. C. *Principles of Molecular Photochemistry: An Introduction*; University Science Books: Sausalito, CA, 2009.

(23) Alberding, B. G.; Chisholm, M. H.; Gustafson, T. L. *Inorg. Chem.* **2012**, *51*, 491−498.

(24) Alberding, B. G.; Brown-Xu, S. E.; Chisholm, M. H.; Gallucci, J. C.; Gustafson, T. L.; Naseri, V.; Reed, C. R.; Turro, C. *Dalton Trans.* **2012**, *41*, 12270−12281.

(25) Brown-Xu, S. E.; Chisholm, M. H.; Durr, C. B.; Spilker, T. F. *J. Am. Chem. Soc.* **2013**, *135*, 8254−8259.

(26) Brignole, A. B.; Cotton, F. A. *Inorg. Synth.* **1972**, *13*, 81−89.

(27) Suzuki, T.; Ota, Y.; Kasuya, Y.; Mutsuga, M.; Kawamura, Y.; Tsumoto, H.; Nakagawa, H.; Finn, M. G.; Miyata, N. *Angew. Chem., Int. Ed.* **2010**, *49*, 6817−6820.

(28) Frisch, M. J.; Trucks, G. W.; Schlegel, H. B.; Scuseria, G. E.; Robb, M. A.; Cheeseman, J. R.; Scalmani, G.; Barone, V.; Mennucci, B.; Petersson, G. A.; Nakatsuji, H.; Caricato, M.; Li, X.; Hratchian, H. P.; Izmaylov, A. F.; Bloino, J.; Zheng, G.; Sonnenberg, J. L.; Hada, M.; Ehara, M.; Toyota, K.; Fukuda, R.; Hasegawa, J.; Ishida, M.; Nakajima, T.; Honda, Y.; Kitao, O.; Nakai, H.; Vreven, T.; Montgomery, Jr., J. A.; Peralta, J. E.; Ogliaro, F.; Bearpark, M.; Heyd, J. J.; Brothers, E.; Kudin, K. N.; Staroverov, V. N.; Kobayashi, R.; Normand, J.; Raghavachari, K.; Rendell, A.; Burant, J. C.; Iyengar, S. S.; Tomasi, J.; Cossi, M.; Rega, N.; Millam, N. J.; Klene, M.; Knox, J. E.; Cross, J. B.; Bakken, V.; Adamo, C.; Jaramillo, J.; Gomperts, R.; Stratmann, R. E.; Yazyev, O.; Austin, A. J.; Cammi, R.; Pomelli, C.; Ochterski, J. W.; Martin, R. L.; Morokuma, K.; Zakrzewski, V. G.; Voth, G. A.; Salvador, P.; Dannenberg, J. J.; Dapprich, S.; Daniels, A. D.; Farkas, O.; Foresman, J. B.; Ortiz, J. V.; Cioslowski, J.; Fox, D. J. *Gaussian 09, Revision A.1*; Gaussian, Inc.: Wallingford, CT, 2009.

(29) Parr, R. G.; Yang, W. *Density Functional Theory of Atoms and Molecules*; Oxford University Press: New York, 1989.

(30) Miehlich, B.; Savin, A.; Stoll, H.; Preuss, H. *Chem. Phys. Lett.* **1989**, *157*, 200−206.

(31) Dennington, R., II; Keith, T.; Millam, J.; Eppinnett, K.; Hovell, W. L.; Gilliland, R. *GaussView*; Semichem Inc: Shawnee Mission, KS, 2003.

(32) Sheldrick, G. M. *SADABS, v2008/1 semi-empirical absorption and beam correction program*; University of Gottingen: Germany.

(33) Sheldrick, G. *Acta Crystallogr.* **2008**, *A64*, 112−122.

(34) Farrugia, L. *J. Appl. Crystallogr.* **1999**, *32*, 837−838.

(35) Wilson, A. J. C.; Geist, V. *International Tables for Crystallography, Vol. C*; Kluwer Academic Publishers: Dordrecht, Netherlands, 1992.

(36) Burdzinski, G.; Hackett, J. C.; Wang, J.; Gustafson, T. L.; Hadad, C. M.; Platz, M. S. *J. Am. Chem. Soc.* **2006**, *128*, 13402−13411.

(37) Wang, J.; Burdzinski, G.; Kubicki, J.; Platz, M. S. *J. Am. Chem. Soc.* **2008**, *130*, 11195−11209.

(38) Byrnes, M. J.; Chisholm, M. H.; Gallucci, J. A.; Liu, Y.; Ramnauth, R.; Turro, C. *J. Am. Chem. Soc.* **2005**, *127*, 17343−17352.